*Journal of Thermal Analysis and Calorimetry, Vol. 59 (2000) 157–168*

*Dedicated to Prof. Edith A. Turi in recognition of her leadership in education*

# THE EFFECT OF SIDE CHAIN ASSOCIATION ON THERMAL AND VISCOELASTIC PROPERTIES
## Cellulose acetate based polycaprolactones

*H. Hatakeyama*[1], *T. Yoshida*[1] *and T. Hatakeyama*[2*]

[1]Fukui Institute of Technology, 3-6-1 Gakuen, Fukui, 910-8505
[2]Otsuma Women's University, 12 Sanban-cho, Chiyoda-ku, Tokyo, 102-8357 Japan

## Abstract

Cellulose acetate-based polycaprolactones (CAPCL's) were synthesized by the polymerization of ε-caprolactone which was initiated by non-substituted OH group in cellulose acetate. The CL/OH (mol mol$^{-1}$) ratios of the CAPCL's were changed from 2 to 20. Thermal and viscoelastic properties of the CAPCL sheets were studied by differential scanning calorimetry (DSC) and dynamic mechanical analysis (DMA). Glass transition, cold crystallization and melting were determined by DSC. Dynamic modules (*E'*), dynamic loss modules (*E"*) and tanδ were measured in a temperature range from –150 to 50 °C by DMA. Apparent activation energy of a dispersion was calculated from the frequency dependency of *E"* peak temperature. It was found that the main chain motion of both CA and PCL is observed in a CL/OH ratio from 0 to 10 mol mol$^{-1}$. However, when CL/OH ratio exceeds 10 mol mol$^{-1}$, the crystalline region which is rearranged by the PCL chain association is observed and only the main chain motion of PCL can be detected.

**Keywords**: cellulose acetate, DSC, glass transition, melting, polycaprolactone

## Introduction

Cellulose and its derivatives have recently received particular attention due to their biocompatible and biodegradable properties. In our previous studies, the hydroxyl group of plant components was used as an active reaction site for the preparation of various types of biodegradable polymers [1–8]. Recently, saccharide-based and lignin-based polycaprolactones (PCL) were newly synthesized [9, 10]. PCL is known as a representative biodegradable and biocompatible polymer [11, 12], at the same time, the higher order structure can be controlled by suitable thermal treatments [13]. On this account, it is considered that the higher-order structure of cellulose based PCL can be expected to be controlled through appropriate processing.

In this study, polycaprolactone chains of various lengths are introduced to cellulose acetate and phase transition behaviour is investigated by dynamic mechanical

* Author to whom all correspondence should be addressed.

*1418–2874/2000/ $ 5.00*

*Akadémiai Kiadó, Budapest*
*Kluwer Academic Publishers, Dordrecht*

analysis (DMA) and differential scanning calorimetry (DSC). We have paid special attention to the side chain association taking into account the thermal history.

## Experimental

*Sample preparation*

Cellulose acetate (CA, acetyl content, 39.87 %) was obtained from Kodak Co. Ltd. PCL with molecular weight $1.0\times10^4$ was purchased from Wako Pure Chemical Co. Ltd, Japan. CAPCL's were synthesized from CA by the polymerization of ε-caprolactone (CL) which was initiated by the OH group of CA. CL/OH (mol $mol^{-1}$) ratios were varied from 2 to 20 (CL/OH ratio=2, 5, 8, 10, 15 and 20 mol $mol^{-1}$). The polymerization was carried out for 12 h at 150 °C with the presence of a small amount of dibutyltin dilaurate (DBTDL). CAPCL sheets were prepared by heat-pressing the synthesized polymers at 160–180°C at ca. 100 kg $cm^{-2}$. The chemical structure of the sample is shown in Fig. 1.

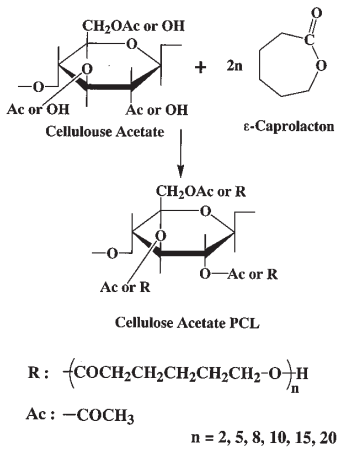


**Fig. 1** Chemical structures of CA based polycaprolactones

*Methods*

DMA

A Seiko dynamic mechanical analyzer DMS 210 equipped with a stretching module was used for the measurement of viscoelastic properties. Sample size was as follows; width 8 mm, length 20 mm and thickness 0.2–0.7 mm. Temperature was varied from –150 to 100–150°C. The maximum temperature was chosen depending on the rigidity of each sample. Liquid nitrogen was used as a coolant and dry nitrogen gas was used as a flowing gas. The heating rate was 2°C $min^{-1}$ . Frequency was varied at 0.1,

1.0, 2.0, 3.0 and 5.0 Hz, respectively. Dynamic modules ($E'$), dynamic loss ($E''$) and tanδ were automatically calculated using the equipped software. Activation energy ($E_a$) of each dispersion was calculated using both automatic calculation software and/or manual calculation.

DSC

Differential scanning calorimetry (DSC) was performed using a Seiko DSC 220C at a heating rate of 10°C min$^{-1}$ under a nitrogen flow (flow rate=30 ml min$^{-1}$). Sample mass was 5–10 mg. Aluminum open pans were used. The samples were heated to 120°C and cooled at 40°C min$^{-1}$ to –120°C. DSC heating curves were measured at 2°C min$^{-1}$ in order to coordinate the heating rate of DMA. DSC curves measured at 10°C min$^{-1}$ were obtained in order to examine the heating rate dependency. The melting temperature ($T_m$), enthalpy of melting ($\Delta H_m$), glass transition temperature ($T_g$) and heat capacity gap at $T_g$($\Delta C_p$) were determined by the method reported previously [13, 14].

TG

Thermogravimetry (TG) was carried out in nitrogen (flow rate=200 ml min$^{-1}$) using a Seiko TG 220 at a heating rate of 20°C min$^{-1}$ in the temperature range from 20 to 800°C. Sample mass was ca. 5 mg. TG curves and derivatograms were recorded.

## Results and discussion

By TG measurements, it was found that the samples used in this study decomposed at a temperature higher than 350°C. Thermal decomposition of the CAPCL's measured by TG-Fourier transform Infrared spectroscopy (TG-FTIR) was reported in detail in our previous report [15]. DSC and DMA measurements were carried out at a temperature where the samples are thermally stable.

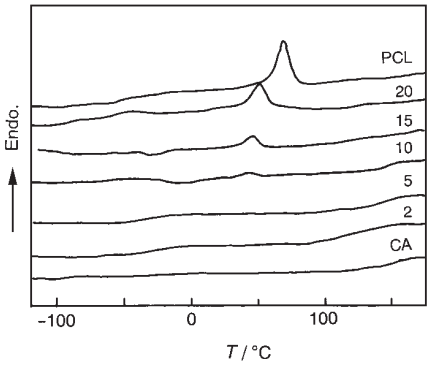


**Fig. 2** Stacked DSC curves of CA amd CAPCL with various CL/OH ratios heated at 10°C min$^{-1}$. Values in the figure show CL/OH ratio

Figure 2 shows stacked DSC curves of CA, PCL and CAPCL's measured at 10°C min$^{-1}$. As shown in Fig. 2, a baseline deviation showing glass transition is clearly observed for CA sample. DSC curves were also measured at various heating rates from 2 to 40°C min$^{-1}$ and heating rate dependency of $T_g$ was clearly observed. It is known that $T_g$ of CA depends mainly on acetyl contents not on molecular weight or molecular weight distribution [16]. $T_g$ of CA observed in this study was 147°C and this value accords well with reported values [16]. Both glass transition and melting can be observed in the DSC curve of PCL. A melting peak was observed at 67°C and $\Delta H_m$ was 88 J g$^{-1}$. This values accords well with reported values [17]. It is reported that $\Delta H_m$ of 100 % crystallinity of PCL is 139.5 J g$^{-1}$ [18]. It is reasonable to detect $T_g$, since the crystallinity of the sample shown in Fig. 2 is ca. 62%.

Melting peak of PCL chains was observed for the PCL samples with CL/OH ratio 10, 15 and mol mol$^{-1}$. A broad exothermic peak due to cold crystallization ($T_{cc}$) at –30°C can be observed for the sample with CL/OH ratio 15 mol mol$^{-1}$. An endothermic peak observed at around 50°C is attributed to the melting of PCL chain. In order to obtain samples having the same thermal history in both DSC and DMA measurements, samples were heated to 120°C and cooled to –150°C at the cooling rate of 40°C min$^{-1}$. The heating run was carried out at 2°C min$^{-1}$. By slow heating, $T_m$ shifted to the high temperature side and $\Delta H_m$ (J g$^{-1}$) increased. $T_m$ of the sample with CL/OH ratio 8 mol mol$^{-1}$ became observable, in contrast, $T_{cc}$ was hardly observed in the samples heated at 2°C min$^{-1}$.

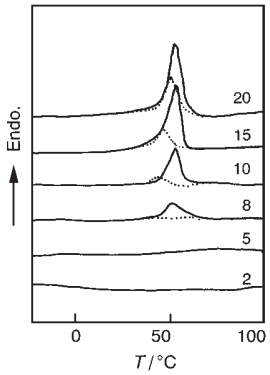


**Fig. 3** Stacked DSC curves of PCL and CAPCL's with various CL/OH ratios heated at 10°C min$^{-1}$. Values in the figure show CL/OH ratio. —– heated at 2°C min$^{-1}$; ····· – at 10°C min$^{-1}$

Figure 3 shows magnified melting curves of CAPCL samples. Temperature of melting ($T_m$) and enthalpy of melting, $\Delta H_m$ (J g$^{-1}$) increase with increasing CL/OH ratio. Both $T_m$ and $\Delta H_m$ of the samples heated at 2°C min$^{-1}$ are higher than those heated at 10°C min$^{-1}$. Figure 4 shows the relationships between $T_m$, $\Delta H_m$ and CL/OH ratio. The results indicate that the higher order structure formation is strongly affected by thermal history, i.e. the crystallinity of PCL chains increases during heating.

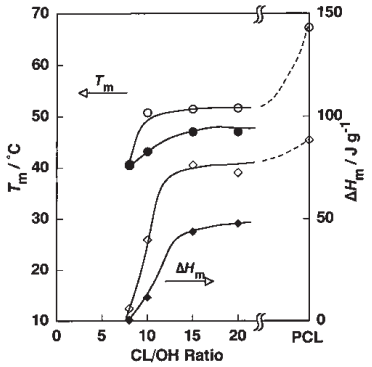


**Fig. 4** Relationships between $T_m$, $\Delta H_m$ and CL/OH ratio; o – $T_m$ of the samples heated at 2°C min$^{-1}$; • – $T_m$ of the samples heated at 10°C min$^{-1}$; ◊ – $\Delta H_m$ of the samples heated at 2°C min$^{-1}$; ♦ –$\Delta H_m$ of the samples heated at 10 °C min$^{-1}$

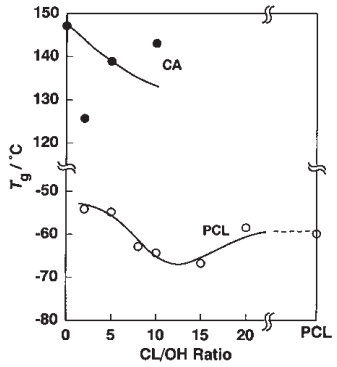


**Fig. 5** Relationships between $T_g$'s and CL/OH ratio. • – CA; o – PCL

It is known that dry cellulose shows no glass transition in a temperature from 20°C to thermal decomposition temperature [19]. Previous studies on heat capacity ($C_p$) measurement of the dry cellulose show that the gradient of $C_p$ increase depends on crystallinity of cellulose [19]. When acetyl group is introduced to the cellulose main chain, $T_g$ can be observed as shown in Fig. 2. The above facts suggest that $T_g$ of glucopyranose ring can be observed by the introduction of large side chain molecules. When DSC curves shown in Fig. 2 are magnified, the two baseline deviations due to glass transition of CA and PCL are observed. $T_g$ of CA can be observed in the initial stage and becomes difficult to detect when CL/OH ratio exceeds 15 mol mol$^{-1}$. It is thought that $T_g$ of CA is observable when intermolecular distance expands by the introduction of large side chain molecules, and the geometrical free space enhances the main chain motion of the main chain. $T_g$ of PCL decreases in the initial stage and increases slightly after reaching a minimum point at around CL/OH= 10 mol mol$^{-1}$. $T_g$ increase observed in the sample with CL/OH ratio 20 suggests that the molecular

motion of PCL random chains is restricted by the presence of crystalline region. Figure 5 shows relationships between $T_g$'s and CL/OH ratio.

The heat capacity difference at $T_g$ ($\Delta C_p$) varies inversely with $T_g$ and the highest value of $\Delta C_p$ is observed at around CL/OH ratio 10 mol mol$^{-1}$. The variation of $T_g$ shown in Fig. 6 suggests that the main chain motion of PCL is enhanced with increasing chain length. At the same time, if PCL long chain molecules form a well arranged crystalline structure molecular motion of the main chain is restricted. It is known a variety of side chain type polymer liquid crystal form various liquid crystalline states by the association of side chains [20, 21]. It is also known that the non-crystalline state coexists with the liquid crystalline state, and that the relative content of each component varies with the thermal treatment [22].

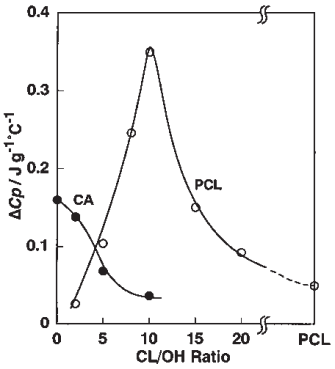


**Fig. 6** Relationships between $\Delta C_p$ and CL/OH ratio. • – CA; o – PCL

It is known that a reciprocal relationship is established between $T_g$ and $\Delta C_p$ values among a large number of amorphous polymers when the samples are completely random and have no intermolecular bonding [23, 24], When the relationship between $T_g$ and $\Delta C_p$ is discussed for complex polymers, such as CAPCL, it must be taken into consideration that the thermodynamically equilibrium state is not attained in either glassy or rubbery state when $\Delta C_p$ values are measured by dynamic measurement. As shown in Figs 2, 3 and 4, the crystalline region is formed in the samples with high CL/OH ratio. A part of the amorphous region is transformed to the crystalline region which can be observed as $T_{cc}$. This means that molecular motion at a temperature higher than $T_g$ of the samples with high CL/OH ratio is restricted and $\Delta C_p$ is necessarily small. The fact that $\Delta C_p$ values cannot be estimated for the samples heated at 2°C min$^{-1}$ indicates that the number of chain molecules contributing to the molecular enhancement is reduced by slow heating. At the same time, a part of the main chain still forms a random structure whose molecular arrangement is similar to that measured at 10°C min$^{-1}$, since a small baseline inflection can be observed and $T_g$ values show no large difference among the samples having different thermal histories.

Figure 7 shows representative DMA heating curves of CAPCL with CL/OH ratio 5 mol mol$^{-1}$ measured at various frequencies. Dynamic modules $E$' (Pa) gradually

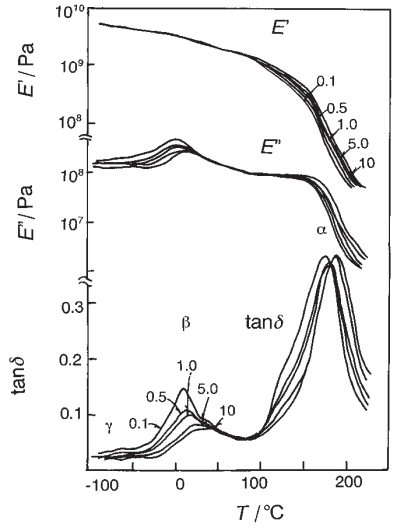


**Fig. 7** DMA curves of CAPCL's with CL/OH ratio=5 mol mol$^{-1}$ at various frequencies. Values show frequency

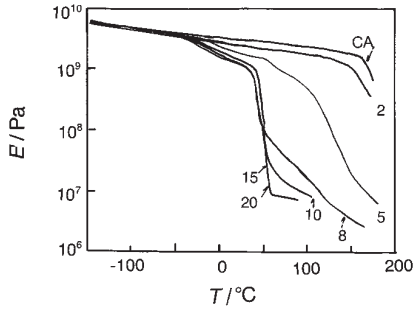


**Fig. 8** Stacked *E*' curves of CA and CAPCL's with various CL/OH ratios. Values show CL/OH ratio mol mol$^{-1}$

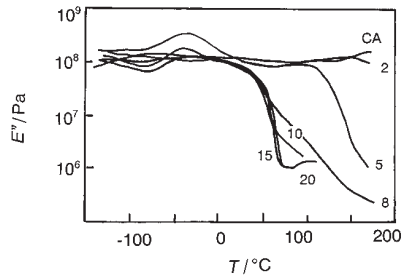


**Fig. 9** Stacked *E*'' curves of CA and CAPCL's with various CL/OH ratios. Values show CL/OH ratio mol mol$^{-1}$

decreases to –50°C and a steep decrease is observed at around 100°C. Dynamic loss modules (*E*") shows three peaks at around –120, –50 and 100°C depending on frequencies. tanδ also shows three peaks. From the high to low temperature side, each *E*" and tanδ peak was designated as α-dispersion, β-dispersion and γ-dispersion, respectively.

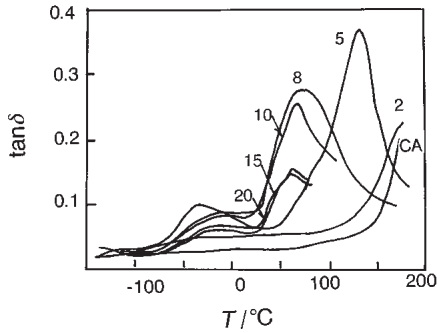


**Fig. 10** Stacked tanδ curves of CA and CAPCL's with various CL/OH ratios. Values show CL/OH ratio mol mol$^{-1}$

Figures 8, 9 and 10 show stacked *E*', *E*" and tanδ curves of CA and CAPCL samples having various DL/OH ratios measured at 1.0 Hz. As shown in Fig. 8, *E*' of CA and CAPCL with CL/OH ratio 2 mol mol$^{-1}$ maintains on almost constant value until 120°C and slightly decreases at a temperature higher than 120°C. The decrease is α-dispersion attributed to $T_g$ of CA. *E*' steeply decreases at around 50°C for CAPCL samples which show melting peak in DSC curves. Ordinarily, it is difficult to measure melting by DMA due to the change of sample shape. However, in this case, CA takes a role of support of PCL and melting of PCL is observed by DMA. A slight decrease of *E*' is observed at around –50°C and this corresponds to β-dispersion. β-dispersion is attributed to $T_g$ of PCL. Dynamic loss *E*" (Fig. 9) and tanδ (Fig. 10) show α- and β-dispersion. Moreover, γ-dispersion is observed as a small peak at around –120°C for CA and CAPCL with a low CL/OH ratio.

Figure 11 shows peak temperature of *E*" (Pa) ($T_a$), the temperature as a function of CL/OH ratio. $T_g$ determined by DSC is also shown. From the above figure, it is reasonable to consider that both temperatures should be attributed to the same molecular movement.

When the chain length of PCL increases, β-dispersion becomes marked i.e. intensities of *E*" and tanδ increase and decrease after reaching the maximum. The variation corresponds to the number of amorphous chains concerning β-dispersion. When the crystalline region is formed, the crystallites restrict the incoherent movement of random chains and the number of molecular chains involving molecular enhancement decreases. Figure 12 shows the change of intensities of *E*" (Pa) and tanδ at the peak temperature with CL/OH ratio. Both values show a maximum at around CL/OH =8 to 10 mol mol$^{-1}$. The variation of the intensities of *E*" and tanδ at the β-dispersion shown in Fig. 12 is similar to

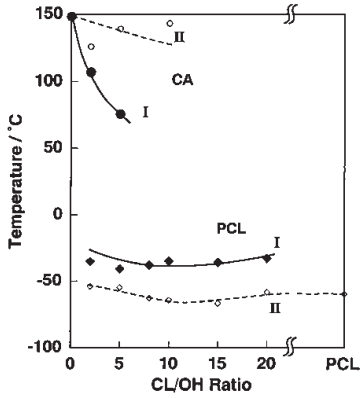


**Fig. 11** Relationships between temperature of I – $E$" maximum, II – $T_g$ and CL/OH ratio

that of $\Delta C_p$ shown in Fig. 6. Both results indicate that the molecular mobility of the main chains is high at around CL/OH ratio 5–10 mol mol$^{-1}$. When either the side PCL chain length is short or the crystallinity increases, free molecular motion is disturbed.

Activation energy ($E_a$) of each dispersion was calculated from frequency dependence of maximum temperature of $E$" assuming the applicability of Arrhenius equation. Figure 13 shows the relationships between frequency and reciprocal maximum temperature of β-dispersions of CAPCL's.

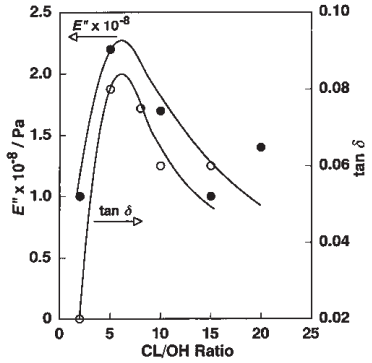


**Fig. 12** Relationship between intensity of $E"_{max}$ and $\tan\delta_{max}$

Activation energies ($E_a$'s) were calculated from the gradient of each line. $E_a$ of β-dispersion is shown in Fig. 14, $E_a$ reaches a minimum at around CL/OH ratio =8 mol mol$^{-1}$. As already reported, $E_a$ of the main chain motion ranges from 100 to 250 J mol$^{-1}$ [25]. It is appropriate to consider that β-dispersion is attributed to the main chain motion of PCL side chain.

The fact that the maximum temperature values obtained by DMA are higher than the $T_g$'s obtained by DSC is explained as follows. If the lines shown in Fig. 13 are extrapolated to $E''$ maximum values, the frequencies where $T_g$'s are observed by DSC can be estimated. Extrapolated values were ranged in $10^{-3}$ to $10^{-4}$ Hz, although

the data were distributed. In our previous study on the heat capacity of cellulose, the frequency of vibration, ca $1.3\times10^{-3}$, of the crystalline cellulose was calculated and that of the amorphous cellulose was ca. $9.1\times10^{-4}$ [19]. It is thought that the estimated values in this study range within the values estimated by the heat capacity calculation. This suggests that DSC measurements correspond to low frequency measurement by DMA.

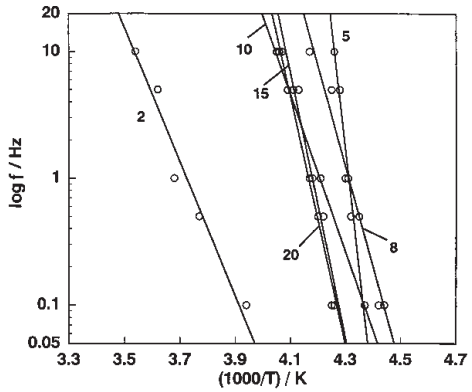


**Fig. 13** Relationships between log $f$ and $T^{-1}$ of CAPCL with various CL/OH ratios. Values show CL/OH ratio in mol mol$^{-1}$

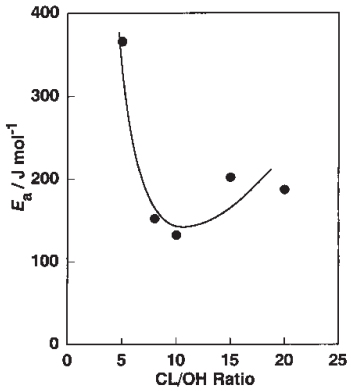


**Fig. 14** Relationship between $E_a$ (activation energy α dispersion) of and CL/OH ratio

From the above results, it can be said that the main chain motion of both CA and PCL chains is observed in a CL/OH ratio 2–10 mol mol$^{-1}$. PCL chains attached to glucopyranose rings were associated with each other at around CL/OH ratio 8 mol mol$^{-1}$, and the melting of the crystalline region of PCL chains can be observed at around 55°C. The main chain motion of CA can be observable in a low CL/OH ratio, however, it becomes difficult to detect when the crystalline region of PCL is formed. Variation of $T_g$, temperature of β-dispersion of PCL and $\Delta C_P$ indicates that

the molecular chains become mobile with increasing CL/OH ratio until CL/OH reaches 10 mol mol$^{-1}$. After that the main chain motion of PCL is restricted by crystal growth, since sufficiently long chains are assembled to form a crystalline region. The sample with CL/OH ratio 5–10 shows intermediate characteristics, i.e. amorphous structure is formed by cooling from the molten state and cold crystallization is observed during heating. However, when the sample is slowly heated, crystallites were formed. On this account, the difference between $T_m$ of samples having different heating rates was observed. This suggests that amorphous content and/or crystallinity can be controlled by suitable thermal treatment. This indicates that the degree of freedom of molecular chains decreases with crystal growth. By the comparison of DSC and DMA results, it can be said that molecular motion measured by DSC corresponds to that measured at low frequency range by DMA.

## References

1 K. Nakamura, T. Hatakeyama and H. Hatakeyama, Polym. Adv. Technol., 3 (1992) 151.
2 K. Nakamura, Y. Nishimura, T. Hatakeyama and H. Hatakeyama, Proceedings for International Workshop on Environmentally Compatible Materials and Recycling Technology in Tsukuba, Japan, November 15–16 (1993), p. 239.
3 H. Hatakeyama, S. Hirose, K. Nakamura and T. Hatakeyama, in Cellulosics: Chemical, Biochemical and Material Aspects, J. F. Kennedy, G. O. Phillips and P. A. Williams, Eds., Ellis Horwood, 1993 p. 381.
4 H. Yoshida, K. Kobashigawa, S. Hirose and H. Hatakeyama, Workshop on Environmentally Compatible Materials and Recycling Technology in Tsukuba, Japan, November (1993), p. 15.
5 M. J. Donnely, Polymer International, 37 (1995) 297.
6 N. Morohoshi, S. Hirose, H. Hatakeyama, T. Tokashiki and K. Teruya, Sen-i Gakkaishi, 51 (1995) 143.
7 K. Nakamura, Y. Nishimura, P. Zetterlund, T. Hatakeyama and H. Hatakeyama, Thermochim. Acta, 43 (1996) 282.
8 P. Zetterlund, S. Hirose, T. Hatakeyama, H. Hatakeyama and A.-C. Albertsson, Polym. Int., 42 (1997) 883.
9 H. Hatakeyama, Y. Izuta, K. Kobashigawa, S. Hirose and T. Hatakeyama, Macromol. Symp., 130 (1998) 127.
10 T. Hatakeyama, T. Tokashiki and H. Hatakeyama, Macromol. Symp., 130 (1998) 139.
11 C. Miola, T. Hamaide and R. Spitz, Polym., 38 (1977) 5667.
12 C. de Kese, C. V. Wauven and C. David, Polym. Degrad. Stabil., 55 (1997) 107.
13 S. Slomkowski, Macromol. Symp., 103 (1996) 213.
14 T. Hatakeyama and F. X. Quinn, Thermal Analysis, John Wiley & Sons, Chichester 1994, p. 65.
15 T. Yoshida, H. Hatakeyama, S. Hirose and T. Hatakeyema, Proceedings for Cellulon'99, Tsukuba, Japan, March (1999).
16 K. Kamide and M. Sato, Polym. J., 17 (1985) 919.
17 C. G. Pitt, Biodegradable Polymers and Drug Delivery Systems, Eds. M. Chasin, R. Langer, Marcel Dekker Inc. New York 1990, chp. 3, p. 81.
18 C. G. Pitt, F. I. Chasalow, Y. M. Hibionada, D. M. Klimas and A. Schindler, J. Appl. Polym. Sci., 26 (1981) 3779.

19 T. Hatakeyama, K. Nakamura and H. Hatakeyama, Polym., 23 (1982) 1801.
20 E. T. Samulski, in Physical Properties of Polymers, Am. Chem. Soc. (1993) Chap. 5.
21 E. J. Coles and R. Simon, (ed. A. Blumstein), Polymeric Liquid Crystals, Plenum, New York 1983, p. 351
22 T. Hatakeyama and Z. Liu, in Handbook of Thermal Analysis, John Wiley, Chichester 1998, p. 89.
23 S. Ichihara, Netsu Sokutei no Shinpo, 4 (1986).
24 T. Hatakeyama and H. Hatakeyama, Thermochim. Acta (in press).
25 T. Hatakeyama and Z. Liu, in Handbook of Thermal Analysis, John Wiley, Chichester 1998, p. 206–210.